



Published in final edited form as:

*Biochemistry*. 2013 August 13; 52(32): 5365–5371. doi:10.1021/bi400592d.

## Determining inter-domain structure and dynamics of a retroviral capsid protein in the presence of oligomerization: implication for structural transition in capsid assembly

Kang Chen and Nico Tjandra\*

Laboratory of Molecular Biophysics, Biochemistry and Biophysics Center, National Heart, Lung, and Blood Institute, National Institutes of Health, Bethesda, MD 20892.

### Abstract

Capsid (CA) proteins from all retroviruses, including HIV-1, are structurally homologous dual-domain helical proteins. They form a capsid lattice composed of unitary symmetric CA hexamers. X-ray crystallography has shown that within each hexamer a monomeric CA adopts a single conformation where most helices are parallel to the symmetry axis. In solution large differences in averaged NMR spin relaxation rates for the two domains were observed, suggesting they are dynamically independent. One relevant question for the capsid assembly remains, whether the inter-domain conformer within a hexamer unit needs to be induced or pre-exists within the conformational space of a monomeric CA. The latter seems more consistent with the relaxation data. However, possible CA protein oligomerization and the structure of each domain will affect relaxation measurements and data interpretation. Here using CA proteins from Equine Infectious Anemia Virus (EIAV) as an example, we demonstrate a linear-extrapolation approach to obtain backbone  $^{15}\text{N}$  spin relaxation time ratios  $T_1/T_2$  for a monomeric EIAV-CA in the presence of oligomerization equilibrium. The inter-domain motion turns out to be limited. The large difference in the domain averaged  $\langle T_1/T_2 \rangle$  for a CA monomer is a consequence of the orthogonal distributions of helices in the two domains. The new monomeric inter-domain conformation in solution is significantly different from that in CA hexamer. Therefore if capsid assembly follows a nucleation-propagation process, the inter-domain conformational change might be a key step during the nucleation, as the configuration in hexagonal assembly is never formed by diffusion of its two domains in solution.

---

Large proteins (> 20 kDa) may consist of multiple domains. Individual domains can function as a scaffold or catalytic unit so that the full-length protein is more efficient in serving as a structural component or performing an enzymatic reaction, or both.(1) A retroviral capsid (CA) protein, consisting of two helical domains, is a typical example of the utilization of both domains to assemble a dense core to protect the retroviral genomic RNA in complex with the nucleocapsid (NC) protein. CA and NC proteins, in addition to matrix (MA) protein, are the three major proteolytic products of the precursor Gag poly-protein formed during viral maturation. CA proteins from all species of retroviruses are 26-27 kDa in size and structurally homologous.(2) X-ray crystallography and cryo-Electron-

---

\*Corresponding Author Tel: (301)-402-3029; Tjandran@nhlbi.nih.gov.

Microscopy (EM) structures of CA proteins from N-tropic murine leukaemia virus (N-MLV),(3) HIV-1,(4-6) and Rous Sarcoma Virus (RSV)(7) have revealed that the outer-layer of the capsid core is composed of a hexagonal and pentagonal assembly of the 7-helix CA N-terminal domain (CA<sup>N</sup>) and the inner-layer is formed through dimerization of neighboring hexamers by the 4-helix C-terminal domain (CA<sup>C</sup>). The inter-domain conformation within all known CA assembly is unique and most helices, helices  $\alpha$ 1-3 and  $\alpha$ 7 of the CA<sup>N</sup> and helices  $\alpha$ 8-11 of the CA<sup>C</sup>, are parallel to the hexamer symmetric axis. Though the inter-domain structure of CA is available for the assembled lattice, the assembly process of CA itself is dynamic and less understood.(8) The proteolysis cleavage of Gag poly-protein, a process that has been targeted by HIV-1 drug, regulates the release of CA, but may or may not be directly related to the CA assembly.(9, 10) Structure and dynamics studies of CA in solution can perhaps address a relevant question whether the assemble ready conformer has to be induced from or is already pre-existing in its monomer state in solution. Analogous to helix-coil transition(11) or protein-ligand conformational switch,(12) if a retroviral capsid assembly has to be induced, other factors, *e.g.* pH or ligand or protein-protein interaction, must be involved to create an activated conformer of CA from its equilibrium state, corresponding to the initial process of nucleation-propagation; in contrary, pre-existing would suggest the assembly starts from a sub-population of assemble ready inter-domain conformer within an equilibrated ensemble of CA structures in solution.

Generally solution NMR can provide inter-domain structural information, *i.e.*, inter-domain NOEs, residual dipolar coupling (RDC),(13-16) and relaxation time ratios  $T_1/T_2$ .(17-22) NOEs are measurable only if the inter-domain contacts involving protons are within a short distance and long lived. Even when these requirements are fulfilled, the NOEs may not be measureable in large proteins, since deuteration maybe required to obtain sharper resonance lines. RDCs are very useful in positioning domains relative to each other. If a multi-domain protein is within oligomerization equilibrium, RDCs are averaged results of all possible oligomers exchanging up to millisecond time scale and are strongly biased toward larger oligomers. RDC data interpretations quickly become difficult if the oligomerization is coupled to inter-domain structural change. The ratio of backbone <sup>15</sup>N spin relaxation times  $T_1/T_2$  is insensitive to fast local dynamics of the amide H-N bond,(23) and reflects the overall rotational diffusion of the domain.(24-27) The average  $T_1/T_2$  values as well as their variation can be used to estimate a domain rotational correlation time and its geometrical shape, respectively. The average  $\langle T_1/T_2 \rangle$  of each domain can be directly used to indicate the presence of inter-domain motion.(28, 29)

The previous solution NMR studies on RSV-CA(28) have suggested that the motion of the two retroviral CA domains are independent of each other based on the lack of inter-domain NOEs and the difference in <sup>15</sup>N  $T_1/T_2$ .(8) This observation is consistent with the pre-existing mechanism for CA assembly. However, CA proteins are likely to be in oligomerization equilibrium through domains CA<sup>N</sup> or CA<sup>C</sup>, and the measured  $T_1/T_2$  might contain contributions from oligomers that can bias the relaxation values for each domain differently. For instance, the CA protein of Equine Infectious Anemia Virus (EIAV), belonging to the same lentivirus subfamily as HIV-1, weakly oligomerize and dimerize through its the CA<sup>N</sup> and CA<sup>C</sup> domains, respectively. And these two equilibriums appear to

be independent processes as a result of the different motional time scales.(30) The assembled EIAV capsid is in the same conical shape as HIV-1 capsid.(31) The study here is to use NMR  $^{15}\text{N}$  relaxation and extrapolation data analysis to overcome oligomerization problem and at the same time to quantitatively reveal if the assemble-ready inter-domain conformer could be present in the conformational space of a monomeric EIAV-CA. Our results showed that the inter-domain structure of EIAV-CA monomer is relatively rigid and different from the assembled structure, and the CA assembly should be induced by other factors.

## Materials and Methods

### Backbone $^{15}\text{N}$ $T_1$ and $T_2$ Measurements

The expression and purification of  $^{15}\text{N}/^2\text{H}$  labeled EIAV-CA protein was described.(30) Four samples at protein concentrations of 0.426, 0.213, 0.106, and 0.053 mM were prepared in a buffer of 20 mM potassium phosphate at pH 6.7. All spin relaxation measurements were performed at 27 °C on a Bruker Avance 600 MHz spectrometer equipped with a cryogenic probe. Pulse sequences with TROSY detection scheme and minimal water saturation were applied.(32) For  $T_1$  measurements eight data points with relaxation delay of 80, 240, 420, 620, 840, 1140, 1460, and 1940 ms were collected. For  $T_{1\rho}$  the  $^{15}\text{N}$  spin lock power was set at 2000 Hz and eight data points with relaxation delay of 2, 7.2, 12.8, 20, 28.8, 39.2, 50.4, and 67.2 ms were collected. Both  $T_1$  and  $T_{1\rho}$  experiments were collected in an interleaved manner. NMRPipe was used to process all spectra.(33) Relaxation time constants and errors were obtained from exponential fitting on peak heights using Sparky (T.D. Goddard and D.G. Kneller, University of California, San Francisco). The calculation of  $T_2$  using  $T_1$  and  $T_{1\rho}$  was previously described.(32)

### Extrapolation and Extended Model Free Fitting of $^{15}\text{N}$ $T_1/T_2$

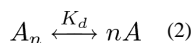
The relaxation time ratios  $T_1/T_2$  at four different protein concentrations were linearly extrapolated. The extrapolated value at the zero concentration was termed  $T_1/T_2$  at “0 mM”. The error of the extrapolated  $T_1/T_2$  was obtained from Monte-Carlo steps. The extended model free (EMF) fitting of  $T_1/T_2$  was carried out as described previously.(34) A fully anisotropic tensor was adopted as the overall rotational diffusion tensor. The domain coordinates were obtained from the crystal structure (35) with the refined  $\beta$ -hairpin motif. (30) The EMF fitting parameters included three principal components of the overall rotational diffusion tensor ( $D_{zz}$ ,  $D_{yy}$  and  $D_{xx}$ ), two sets of Euler angles ( $\alpha$ ,  $\beta$  and  $\gamma$ ) defining the orientation of the overall diffusion tensor within each of the domain coordinates, the domain motion order parameters  $S^2_{\text{domain}}$  and correlation time  $\tau_{\text{domain}}$  that describe the amplitude and time scale of the domain motion within the overall diffusion tensor frame (Table 1). The  $\chi^2$  minimization was against the difference between the measured  $T_1/T_2$  and the calculated values, *i.e.*, Eq. (1), where  $N$  ( $N = 151$ ) the total number of residues used for fitting and  $\delta(T_1/T_2)$  is the experimental error. A simplex searching algorithm written in MATLAB (The Mathworks, MA) was used to locate the global minimal.

$$\chi^2 = \left( \frac{1}{N} \right) \sum_{i=1}^N \left[ \frac{(T_{1i}/T_{2i})_{calc} - (T_{1i}/T_{2i})_{meas}}{\delta(T_{1i}/T_{2i})_{meas}} \right]^2 \quad (1)$$

## Results

### Simulation and Extrapolation on Concentration Dependent $T_1/T_2$

The observation of  $^{15}\text{N}$   $T_1/T_2$  ratios as a function of protein concentration originates from weak protein oligomerization.<sup>(36)</sup> When a protein “A” is in a monomer to oligomer ( $A_n$ ) equilibrium as indicated by Eq. (2), two basic equations, Eq. (3-4), exist, where  $c$  is the total protein concentration,  $K_d$  is the dissociation constant, and  $n$  is the number of monomers within one oligomer. Solving Eq. (3-4) for  $[A]$  and  $[A_n]$  can be performed using Mathematica (Wolfram, IL) for various oligomeric states. For examples, the analytical solutions for  $[A]$  when  $n = 2$  and  $3$  are given in Eq. 5 and 6, respectively. With the knowledge of  $[A]$ , one can readily obtain the population fraction of monomer  $f_A$  in the equilibrium using Eq. (7), and calculate the averaged value  $(T_1/T_2)_{ave}$  according to Eq. (8), where  $(T_1/T_2)_A$  and  $(T_1/T_2)_{An}$  are relaxation times ratios for the monomer and the oligomer, respectively.



$$c = [A] + n[A_n] \quad (3)$$

$$K_d = \frac{[A]^n}{[A_n]} \quad (4)$$

$$[A] = \sqrt{K_d(c/2 + K_d/16)} - K_d/4, n=2 \quad (5)$$

$$[A] = K_d / (27B) - 3B, B = \sqrt[3]{c^3/18 - c(c^2/3 + K_d/27)/6 + \sqrt{K_d^3/531441 + (K_dc/162)^2}}, n=3 \quad (6)$$

$$f_A = \frac{[A]}{c} \quad (7)$$

$$\left( \frac{T_1}{T_2} \right)_{ave} = f_A \left( \frac{T_1}{T_2} \right)_{mono} + (1 - f_A) \left( \frac{T_1}{T_2} \right)_{oligo} \quad (8)$$

Now we consider simulating a system of monomer-dimer ( $n = 2$ ) equilibrium with a weak dissociation constant  $K_d$  of 5 mM, and  $(T_1/T_2)_{mono}$  and  $(T_1/T_2)_{dimer}$  of 10 and 20, respectively. Using Eq. 5, 7, and 8, we calculated and plotted  $(T_1/T_2)_{ave}$  at each

concentrations of 0.05, 0.1, 0.2, and 0.4 mM (Fig. 1A), which were chosen to closely match the current experimental conditions. The linear and quadratic fittings yielded  $(T_1/T_2)_{ave}$ -intercept values of 10.07 and 10.01, respectively. Such intercept values are taken as extrapolated data points, both of which are within 5%, roughly the experimental error range, of the target  $(T_1/T_2)_{mono}$  value of 10. We then fit another system of monomer-trimer ( $n = 3$ ) equilibrium with a weak dissociation constant  $K_d$  of 0.125 mM<sup>2</sup>, and  $(T_1/T_2)_{mono}$  and  $(T_1/T_2)_{trimer}$  of 10 and 30, respectively. Here we have assumed that there are one monomer-monomer interface within a dimer and three interfaces within a trimer, therefore the dissociation constant for the trimer is chosen to correspond to three times the free energy change of the dissociation of the dimer ( $-RT\ln K_d$ ). Using Eq. 6, 7, and 8 we again calculated and plotted  $(T_1/T_2)_{ave}$  at each concentrations of 0.05, 0.1, 0.2, and 0.4 mM (Fig. 1B). The linear and quadratic fittings yielded  $(T_1/T_2)_{ave}$ -intercept values of 10.39 and 8.800, respectively. Only the linear fitting intercept value of 10.39 is within 5% of the targeted  $(T_1/T_2)_{mono}$  value of 10.

Of course our simulation is rudimentary and has a number assumptions. However, it does show that simpler linear fitting could be a more reliable method to obtain monomeric relaxation value when only data from a small number of concentrations are available. This constitutes one reason why we adopted the linear extrapolation for the study.

### Concentration Dependent $T_1/T_2$ of EIAV-CA and its Extrapolation

The <sup>15</sup>N  $T_1/T_2$  ratios were measured at four EIAV-CA concentrations, 0.4, 0.2, 0.1, and 0.05 mM, showing strong concentration dependent for residues in structured region of the protein (Fig. 2 and 3, Table S1). The full-length EIAV-CA protein has a total of 212 non-proline residues. Backbone <sup>1</sup>H-<sup>15</sup>N resonances for 186 residues were assigned and missing residues are I2-M3, R18-T22, I43-E51, M53, N54, G65, Q127, and Y129-I134, which are located along the domain CA<sup>N</sup> oligomeric interfaces. The previous  $R_2$ -CPMG dispersion results demonstrated residues with significant  $\mu$ s-ms exchange contributions are T16, D82, L87 and M102, where the last three are in the cyclophilin A (CypA) binding loop.(30) Those residues undergoing chemical exchange or missing have been removed from the analysis. Further, residues with significantly low signal to noise ratio, yielding large errors in their relaxation times, and the C-terminal flexible residues, displaying no concentration dependence, were removed. Finally 90 and 61 total residues for domains CA<sup>N</sup> and CA<sup>C</sup>, respectively, were left for  $T_1/T_2$  analysis, which were tabulated in the supporting materials (Table S1). To obtain proper <sup>15</sup>N  $T_1/T_2$  for the monomeric EIAV-CA, we applied the linear as well as the quadratic extrapolations using all four sets of  $T_1/T_2$ . For all 151 data points the quadratic fitting did not yield statistically better fitting, judged by the  $F$ -test (data not shown), therefore, only the linear extrapolation was applied (examples of fitting shown in Fig. 3). The obtained new relaxation time ratios from the linear extrapolation were termed  $T_1/T_2$  at “0 mM” and assumed to be the corresponding value in the monomeric state (Fig. 2).

### Empirical Estimation on $\langle T_1/T_2 \rangle$ Yields Large Scale of Inter-Domain Motion

Similar to the previous observations on RSV-CA,(28) the domain averaged  $\langle T_1/T_2 \rangle$  values differ significantly for all measured and the extrapolated datasets (Fig. 2). The size ratio of the domain EIAVCA<sup>N</sup> (residue 1-146) and EIAV-CA<sup>C</sup> (residue 149-220) is 2:1. If the two

domains are completely independent ( $S^2_{\text{domain}} = 0$ ), under the assumptions of isotropic diffusion and isotropic distribution of H-N vectors, the  $\langle T_1/T_2 \rangle$  value of domain CA<sup>C</sup> should be 50% of the  $\langle T_1/T_2 \rangle$  value of domain CA<sup>N</sup>, roughly scaled with the relative domain sizes. For the “0 mM” dataset, the  $\langle T_1/T_2 \rangle$  value of domain CA<sup>C</sup> is 14.86, 66% of the  $\langle T_1/T_2 \rangle$  value of domain CA<sup>N</sup> of 22.26 (Fig. 2). The large difference in domain  $\langle T_1/T_2 \rangle$  suggests the presence of a large-scale inter-domain motion based on the assumption of the isotropic diffusion in each domain.

### Numeric Fitting on $T_1/T_2$ Results in Limited Inter-Domain Motion

We fit the “0 mM”  $T_1/T_2$  dataset using the EMF approach described previously (Table 1). (34) The resulting diffusion anisotropy ( $2D_{zz}/(D_{xx}+D_{yy})$ ) and asymmetry ( $D_{yy}/D_{xx}$ ) are large, 1.84 and 1.69, respectively, indicating the “0 mM”  $T_1/T_2$  values are very sensitive to structure coordinates. The  $S^2_{\text{domain}}$  for both domains are high, 1 and 0.854 for domain CA<sup>N</sup> and CA<sup>C</sup>, respectively, meaning inter-domain motion is limited and the empirically estimated large-scale of domain motion is not correct. The reason for the large difference in domain  $\langle T_1/T_2 \rangle$  is obvious once we rotated and positioned the two domains into the overall diffusion tensor (Fig. 4). It should be noted the simple domain rotation generated structure shown in Fig. 4 only represents a mean inter-domain conformation, not a structure ensemble from any simulated annealing calculations. The helices of domain CA<sup>C</sup> are all perpendicular to the long axis ( $D_{zz}$ ) of the diffusion tensor, sampling the fastest components of the overall motion, in contrast, helices  $\alpha 1-3$ , and  $\alpha 7$  of domain CA<sup>N</sup> run parallel to the long axis, experiencing slower tumbling from  $D_{yy}$  and  $D_{xx}$ . One cross-validation of the domain positioning result is to compare the  $T_1/T_2$  values of the N-terminal  $\beta$ -hairpin residues, representing only 4% of the  $T_1/T_2$  dataset, to the rest of the data. The N-terminal  $\beta$ -hairpin, though well ordered within the domain CA<sup>N</sup>, (37-39) is close in  $T_1/T_2$  values to domain CA<sup>C</sup>. This could only be true if the two domains share the same diffusion tensor and the amide bond vectors of the  $\beta$ -hairpin are oriented similar to helices of domain CA<sup>C</sup> (Fig. 2 and 4).

In parallel the EMF fit for  $T_1/T_2$  values of the 0.4 mM dataset was performed (Table 1). The nearly 4-fold higher  $\chi^2$  value indicates the fitting quality is much worse than the extrapolated “0 mM” dataset. The overall correlation time of 18.6 ns is significantly higher than the monomer value of 13.6 ns. The lower diffusion anisotropy and asymmetry indicate less sensitivity of the 0.4 mM dataset to structural coordinates. The lower anisotropy/asymmetry also suggested a more compact conformer was formed upon oligomerization. The  $S^2_{\text{domain}}$  of CA<sup>C</sup> is higher, indicating even less inter-domain motion in oligomer. The  $D_{zz}$  axes of the fit overall diffusion tensors differ by 2.8° and 4.3° for domains CA<sup>N</sup> and CA<sup>C</sup>, respectively, from those of the monomeric tensor, indicating the oligomer (mostly dimer here) tensor direction is not significantly different from the monomer tensor.

### Validation of $T_1/T_2$ Derived Inter-domain Structure

The new inter-domain conformation obtained using the extrapolated  $T_1/T_2$  is different from that in the crystal structures of monomer EIAV-CA(35) or hexamer structure of HIV-1-CA (Fig. 4). (5) The hexamer is the unit for capsid-assembly of all retroviruses. This inconsistency in the inter-domain conformations prompted us to inspect if the  $T_1/T_2$  derived

inter-domain conformation in solution is a true representation. To further investigate this question, we performed a small angle X-ray scattering (SAXS) experiment at concentration of 0.05 mM. The SAXS profile showed the  $T_1/T_2$  derived CA structure provides a better fit than the crystal structures of either monomer or a monomer unit within a hexamer (Fig. 5). As could be expected, the fit for the  $T_1/T_2$  derived CA structure is not perfect at the long-range distance region, indicating the presence of a tiny population of oligomer even at this diluted concentration.

## Discussion

In summary we have presented a straightforward method to extract the mean inter-domain structure and dynamics information from backbone  $^{15}\text{N}$   $T_1/T_2$  data on a protein undergoing oligomerization. Based on simulations and statistical test we suggested the linear extrapolation, as opposed to a combination of linear and quadratic fittings,(36) should be applied to recover the monomer relaxation data at “0” concentration. If the contribution from protein oligomerization was not removed, the data fitting quality would be worse, meaning less agreement between structural coordinates and measured relaxation data. Worse fitting will also cause errors in the resulting parameters, *i.e.*, the correlation time would be higher; the diffusion tensor anisotropy and asymmetry could be wrong; the inter-domain motion  $S^2_{\text{domain}}$  could be different, perhaps resulting in an inaccurate biological conclusion; the tensor direction might not be representative of the monomer if the oligomer tensor direction is significantly different. As has been shown previously, diffusion tensor anisotropy and asymmetry are a few long-range restraints for protein shape that can be used in NMR structure calculation.(25, 27, 40) Though not being tested here, any inaccuracy in the diffusion tensor can bring errors in refining a monomeric protein structure and domain positioning of a multi-domain protein. In theory we might be able to extend the usage of the precisely measured  $^{15}\text{N}$   $T_1/T_2$  to derive protein quaternary structure of oligomers. However, practical methods to take into account the exchange kinetics if it occurs in the ns timescale are not currently available though theoretical treatments do exist.(41, 42)

Though the inter-domain dynamics we identified on EIAV-CA using EMF method is relatively restricted with a higher order parameter  $S^2_{\text{domain}}$  of 0.85, it should not be deemed as the limit of the EMF method. Previous simulations and measurements suggested the EMF fitting approach could be valid for larger domain motions with  $S^2_{\text{domain}}$  as low as 0.4-0.5, corresponding to a semi-cone angle of  $45^\circ$  in the diffusion in the cone model.(43, 44)

Our structural data has an implication on the nucleation of a retroviral CA assembly. The CA assembly is not an isolated event, which results from the proteolytic processing of its precursor Gag, and rather complicated. The nucleation step in capsid assembly, though generally accepted,(45) has not been clearly demonstrated by any physical observations. In fact the *in vitro* assembly of a cone-shaped HIV-1 capsid using recombinant protein was only successful with a combination of its precursor CA-NC protein and RNA, not CA alone. (46, 47) Further, a close inspection of the recent  $8\text{\AA}$  cryo-EM structure of an immature Mason-Pfizer Monkey Virus (MPMV) CA-NC assembly (PDB id 4ARG) (47) revealed a similar inter-domain orientation to the one in a matured HIV-1-CA hexamer (PDB id 3GV2) (5). The difference lies in a translational movement of the  $\text{CA}^{\text{C}}$  or the  $\text{CA}^{\text{N}}$  domain. These

results might suggest the capsid assembly proceed directly from its assembled proteolytic fragment CA-NC proteins during maturation without major inter-domain re-orientation. Therefore the CA assembly probably does not require the diffusion and the nucleation-propagation in solution. A contrasting view can be made from the fact that only a small fraction of CA molecules processed from Gag were utilized for assembly (48) and the observations of the dual-core HIV-1 virion (49) suggest a CA release and re-assembly with several nucleation centers in solution have to take place. These observations argue against direct CA condensation from lattices of Gag or CA-NC. Our  $T_1/T_2$  derived inter-domain structure suggested that the capsid assembly, if it is occurring in solution, does not start readily from a pre-existing assemble-ready conformer, rather a nucleation step involving at least significant inter-domain structure re-orientation appears to be necessary. This finding implies that factors other than the CA protein itself might play a role in promoting capsid assembly. This is inline with earlier observations where neutral pH and high salt concentration helped nucleation,(50) which had been shown to be important for *in vitro* assembly of tubular lattice using recombinant HIV-1-CA proteins.(45) The essential factors capable of inducing an authentic cone-shaped lattice are not known, but are potential for therapeutic targets.

## Supplementary Material

Refer to Web version on PubMed Central for supplementary material.

## Acknowledgments

We thank Alex Grishaev for measuring SAXS data and Charles Schwieters for help with XPLOR-NIH.

### Funding Sources

No competing financial interests have been declared. The project was funded by the Intramural Research Programs of National Heart, Lung, and Blood Institute of the NIH.

## ABBREVIATIONS

CA	capsid
EIAV	equine infectious anemia virus
EMF	extended model free
NC	nucleocapsid

## REFERENCES

1. Petsko, GA.; Ringe, D. Protein structure and function, New Science; Sinauer Associates. Blackwell Publishing; London Sunderland, MA Oxford: 2004.
2. Turner BG, Summers MF. Structural biology of HIV. J Mol Biol. 1999; 285:1–32. [PubMed: 9878383]
3. Mortuza GB, Haire LF, Stevens A, Smerdon SJ, Stoye JP, Taylor IA. High-resolution structure of a retroviral capsid hexameric amino-terminal domain. Nature. 2004; 431:481–485. [PubMed: 15386017]



4. Ganser-Pornillos BK, Cheng A, Yeager M. Structure of full-length HIV-1CA: a model for the mature capsid lattice. *Cell*. 2007; 131:70–79. [PubMed: 17923088]
5. Pornillos O, Ganser-Pornillos BK, Kelly BN, Hua YZ, Whitby FG, Stout CD, Sundquist WI, Hill CP, Yeager M. X-Ray Structures of the Hexameric Building Block of the HIV Capsid. *Cell*. 2009; 137:1282–1292. [PubMed: 19523676]
6. Byeon IJL, Meng X, Jung JW, Zhao GP, Yang RF, Ahn JW, Shi J, Concel J, Aiken C, Zhang PJ, Gronenborn AM. Structural Convergence between Cryo-EM and NMR Reveals Intersubunit Interactions Critical for HIV-1 Capsid Function. *Cell*. 2009; 139:780–790. [PubMed: 19914170]
7. Cardone G, Purdy JG, Cheng NQ, Craven RC, Steven AC. Visualization of a missing link in retrovirus capsid assembly. *Nature*. 2009; 457:694–698. [PubMed: 19194444]
8. Briggs JAG, Krausslich HG. The Molecular Architecture of HIV. *J Mol Biol*. 2011; 410:491–500. [PubMed: 21762795]
9. Lanman J, Lam TT, Emmett MR, Marshall AG, Sakalian M, Prevelige PE. Key interactions in HIV-1 maturation identified by hydrogen-deuterium exchange. *Nat Struct Mol Biol*. 2004; 11:676–677. [PubMed: 15208693]
10. Ganser-Pornillos BK, Yeager M, Pornillos O. Assembly and Architecture of HIV. *Adv Exp Med Biol*. 2012; 726:441–465. [PubMed: 22297526]
11. Zimm BH, Bragg JK. Theory of the Phase Transition between Helix and Random Coil in Polypeptide Chains. *J Chem Phys*. 1959; 31:526–535.
12. Frauenfelder H, Sligar SG, Wolynes PG. The Energy Landscapes and Motions of Proteins. *Science*. 1991; 254:1598–1603. [PubMed: 1749933]
13. Yuwen T, Post CB, Skrynnikov NR. Domain cooperativity in multidomain proteins: what can we learn from molecular alignment in anisotropic media? *J Biomol Nmr*. 2011; 51:131–150. [PubMed: 21947922]
14. Prestegard JH, Al-Hashimi HM, Tolman JR. NMR structures of biomolecules using field oriented media and residual dipolar couplings. *Q Rev Biophys*. 2000; 33:371–424. [PubMed: 11233409]
15. Dosset P, Hus JC, Marion D, Blackledge M. A novel interactive tool for rigid-body modeling of multi-domain macromolecules using residual dipolar couplings. *J Biomol Nmr*. 2001; 20:223–231. [PubMed: 11519746]
16. Ryabov Y, Fushman D. Analysis of interdomain dynamics in a two-domain protein using residual dipolar couplings together with N-15 relaxation data. *Magn Reson Chem*. 2006; 44:S143–S151. [PubMed: 16823894]
17. Fushman D, Xu R, Cowburn D. Direct determination of changes of interdomain orientation on ligation: Use of the orientational dependence of N-15 NMR relaxation in Abl SH(32). *Biochemistry-US*. 1999; 38:10225–10230.
18. Ryabov YE, Fushman D. A model of interdomain mobility in a multidomain protein. *J Am Chem Soc*. 2007; 129:3315–3327. [PubMed: 17319663]
19. Bruschiweiler R, Liao XB, Wright PE. Long-Range Motional Restrictions in a Multidomain Zinc-Finger Protein from Anisotropic Tumbling. *Science*. 1995; 268:886–889. [PubMed: 7754375]
20. Ulmer TS, Werner JM, Campbell ID. SH3-SH2 domain orientation in Src kinases: NMR studies of *Fyn*. *Structure*. 2002; 10:901–911. [PubMed: 12121645]
21. Ryabov Y, Fushman D. Structural assembly of multidomain proteins and protein complexes guided by the overall rotational diffusion tensor. *J Am Chem Soc*. 2007; 129:7894–7902. [PubMed: 17550252]
22. Ryabov Y, Fushman D. Interdomain mobility in Di-ubiquitin revealed by NMR. *Proteins*. 2006; 63:787–796. [PubMed: 16609980]
23. Kay LE, Torchia DA, Bax A. Backbone Dynamics of Proteins as Studied by N-15 Inverse Detected Heteronuclear Nmr-Spectroscopy - Application to Staphylococcal Nuclease. *Biochemistry-US*. 1989; 28:8972–8979.
24. Palmer AG. NMR characterization of the dynamics of biomacromolecules. *Chem Rev*. 2004; 104:3623–3640. [PubMed: 15303831]
25. Tjandra N, Garrett DS, Gronenborn AM, Bax A, Clore GM. Defining long range order in NMR structure determination from the dependence of heteronuclear relaxation times on rotational diffusion anisotropy. *Nat Struct Biol*. 1997; 4:443–449. [PubMed: 9187651]

26. Ryabov Y, Clore GM, Schwieters CD. Direct Use of N-15 Relaxation Rates as Experimental Restraints on Molecular Shape and Orientation for Docking of Protein-Protein Complexes. *J Am Chem Soc.* 2010; 132:5987. [PubMed: 20392103]
27. Ryabov Y, Suh JY, Grishaev A, Clore GM, Schwieters CD. Using the Experimentally Determined Components of the Overall Rotational Diffusion Tensor To Restrain Molecular Shape and Size in NMR Structure Determination of Globular Proteins and Protein-Protein Complexes. *J Am Chem Soc.* 2009; 131:9522–9531. [PubMed: 19537713]
28. Campos-Olivas R, Newman JL, Summers MF. Solution structure and dynamics of the Rous sarcoma virus capsid protein and comparison with capsid proteins of other retroviruses. *J Mol Biol.* 2000; 296:633–649. [PubMed: 10669613]
29. de Alba E. Structure and Interdomain Dynamics of Apoptosis-associated Speck-like Protein Containing a CARD (ASC). *J Biol Chem.* 2009; 284:32932–32941. [PubMed: 19759015]
30. Chen K, Piszczek G, Carter C, Tjandra N. The Maturation Refolding of the beta-Hairpin Motif of Equine Infectious Anemia Virus Capsid Protein Extends Its Helix alpha 1 at Capsid Assembly Locus. *J Biol Chem.* 2013; 288:1511–1520. [PubMed: 23184932]
31. Roberts MM, Oroszlan S. The Preparation and Biochemical-Characterization of Intact Capsids of Equine Infectious-Anemia Virus. *Biochemical and Biophysical Research Communications.* 1989; 160:486–494. [PubMed: 2541703]
32. Chen K, Tjandra N. Water proton spin saturation affects measured protein backbone N-15 spin relaxation rates. *J Magn Reson.* 2011; 213:151–157. [PubMed: 22015249]
33. Delaglio F, Grzesiek S, Vuister GW, Zhu G, Pfeifer J, Bax A. Nmrpipe - a Multidimensional Spectral Processing System Based on Unix Pipes. *Journal of Biomolecular Nmr.* 1995; 6:277–293. [PubMed: 8520220]
34. Baber JL, Szabo A, Tjandra N. Analysis of slow interdomain motion of macromolecules using NMR relaxation data. *J Am Chem Soc.* 2001; 123:3953–3959. [PubMed: 11457145]
35. Jin ZM, Jin L, Peterson DL, Lawson CL. Model for lentivirus capsid core assembly based on crystal dimers of EIAV p26. *J Mol Biol.* 1999; 286:83–93. [PubMed: 9931251]
36. Jensen MR, Kristensen SM, Keeler C, Christensen HEM, Hodsdon ME, Led JJ. Weak self-association of human growth hormone investigated by nitrogen-15 NMR relaxation. *Proteins.* 2008; 73:161–172. [PubMed: 18409193]
37. Gitti RK, Lee BM, Walker J, Summers MF, Yoo S, Sundquist WI. Structure of the amino-terminal core domain of the HIV-1 capsid protein. *Science.* 1996; 273:231–235. [PubMed: 8662505]
38. Macek P, Chmelik J, Krizova I, Kaderavek P, Padrta P, Zidek L, Wildova M, Hadravova R, Chaloupkova R, Pichova I, Ruml T, Rumlova M, Sklenar V. NMR Structure of the N-Terminal Domain of Capsid Protein from the Mason-Pfizer Monkey Virus. *J Mol Biol.* 2009; 392:100–114. [PubMed: 19527730]
39. Cornilescu CC, Bouamr F, Carter C, Tjandra N. Backbone N-15 relaxation analysis of the N-terminal domain of the HTLV-I capsid protein and comparison with the capsid protein of HIV-1. *Protein Sci.* 2003; 12:973–981. [PubMed: 12717020]
40. Ryabov YE, Geraghty C, Varshney A, Fushman D. An efficient computational method for predicting rotational diffusion tensors of globular proteins using an ellipsoid representation. *J Am Chem Soc.* 2006; 128:15432–15444. [PubMed: 17132010]
41. Ryabov Y, Clore GM, Schwieters CD. Coupling between internal dynamics and rotational diffusion in the presence of exchange between discrete molecular conformations. *J Chem Phys.* 2012; 136
42. Wong V, Case DA, Szabo A. Influence of the coupling of interdomain and overall motions on NMR relaxation. *P Natl Acad Sci USA.* 2009; 106:11016–11021.
43. Chang SL, Szabo A, Tjandra N. Temperature dependence of domain motions of calmodulin probed by NMR relaxation at multiple fields. *J Am Chem Soc.* 2003; 125:11379–11384. [PubMed: 16220961]
44. Chen K, Tjandra N. Extended model free approach to analyze correlation functions of multidomain proteins in the presence of motional coupling. *J Am Chem Soc.* 2008; 130:12745–12751. [PubMed: 18761455]

45. Barklis E, Alfadhli A, McQuaw C, Yalamuri S, Still A, Barklis RL, Kukull B, Lopez CS. Characterization of the In Vitro HIV-1 Capsid Assembly Pathway. *J Mol Biol.* 2009; 387:376–389. [PubMed: 19356593]
46. Ganser BK, Li S, Klishko VY, Finch JT, Sundquist WI. Assembly and analysis of conical models for the HIV-1 core. *Science.* 1999; 283:80–83. [PubMed: 9872746]
47. Bharat TAM, Davey NE, Ulbrich P, Riches JD, de Marco A, Rumlova M, Sachse C, Ruml T, Briggs JAG. Structure of the immature retroviral capsid at 8 angstrom resolution by cryo-electron microscopy. *Nature.* 2012; 487:385–389. [PubMed: 22722831]
48. Briggs JAG, Simon MN, Gross I, Krausslich HG, Fuller SD, Vogt VM, Johnson MC. The stoichiometry of Gag protein in HIV-1. *Nat Struct Mol Biol.* 2004; 11:672–675. [PubMed: 15208690]
49. Briggs JAG, Wilk T, Welker R, Krausslich HG, Fuller SD. Structural organization of authentic, mature HIV-1 virions and cores. *Embo J.* 2003; 22:1707–1715. [PubMed: 12660176]
50. Ehrlich LS, Agresta BE, Carter CA. Assembly of Recombinant Human-Immunodeficiency-Virus Type-1 Capsid Protein In Vitro. *J Virol.* 1992; 66:4874–4883. [PubMed: 1629958]
51. Schwieters CD, Kuszewski JJ, Tjandra N, Clore GM. The Xplor-NIH NMR molecular structure determination package. *Journal of Magnetic Resonance.* 2003; 160:65–73. [PubMed: 12565051]

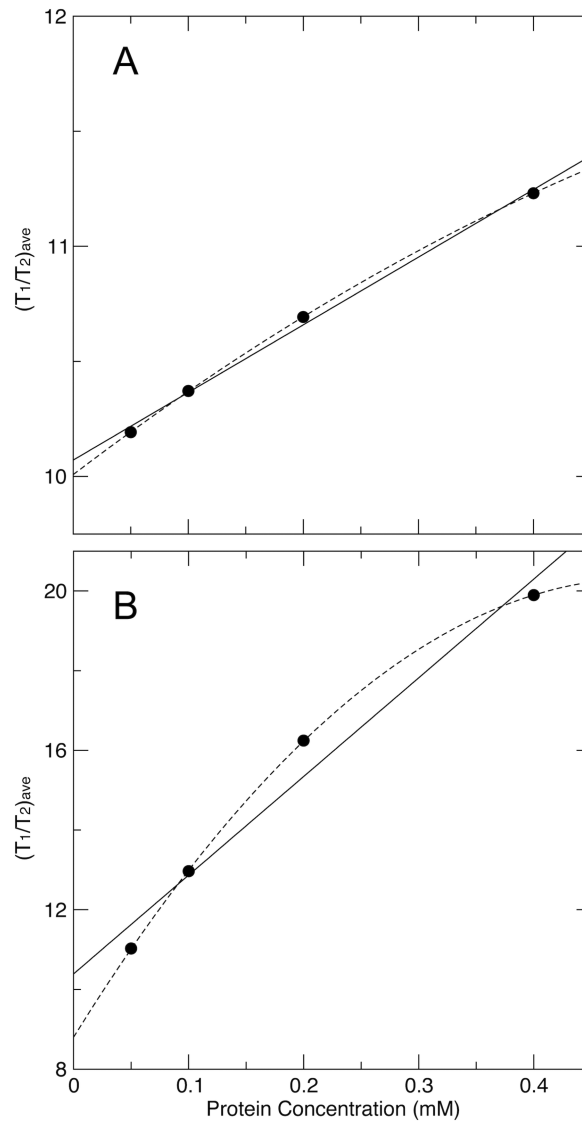


**Figure 1.** The linear (solid lines) and quadratic (dashed lines) fittings on simulated  $(T_1/T_2)_{ave}$  data points (solid dots) under weak dimerization (A) and trimerization (B) equilibriums. The target  $(T_1/T_2)_{ave}$ -intercept value is 10.

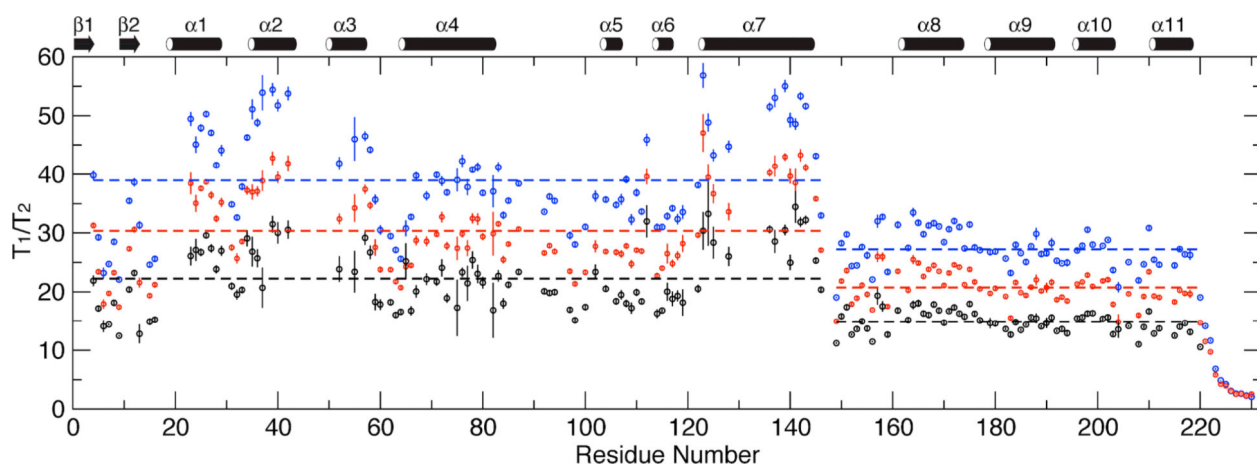


**Figure 2.**

The measured (for clarity only the 0.4 mM and 0.2 mM datasets are shown in blue and red, respectively) and the extrapolated (“0” mM, black) backbone  $^{15}\text{N}$  spin relaxation time ratios  $T_1/T_2$ . The dashed lines mark the average  $\langle T_1/T_2 \rangle$  for each domain in each measurement and end at domain boundaries.

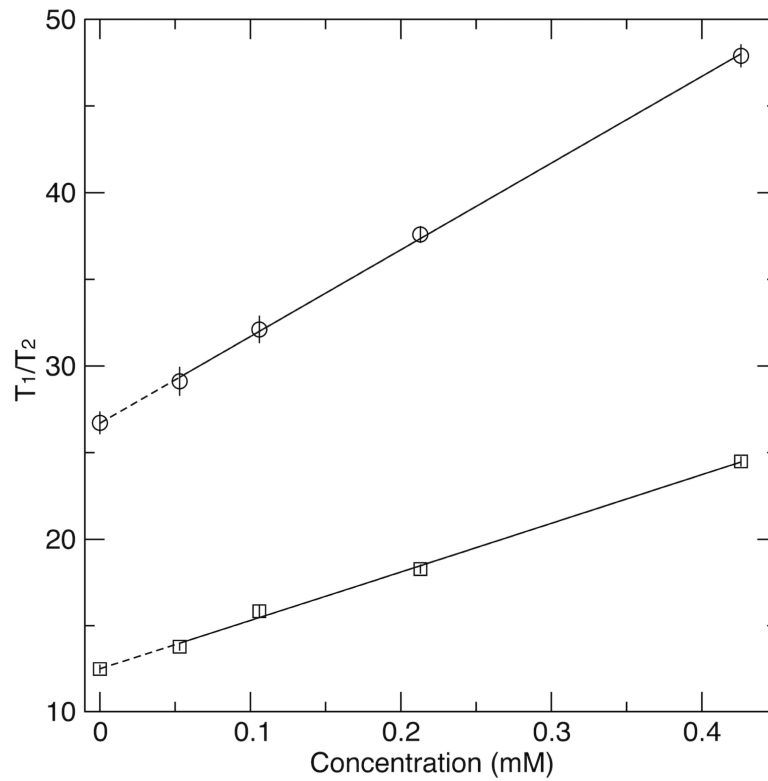


**Figure 3.** Examples of linear extrapolation. The  $T_1/T_2$  ratios are plotted as a function of protein concentration for N25 (circle) and M215 (square).

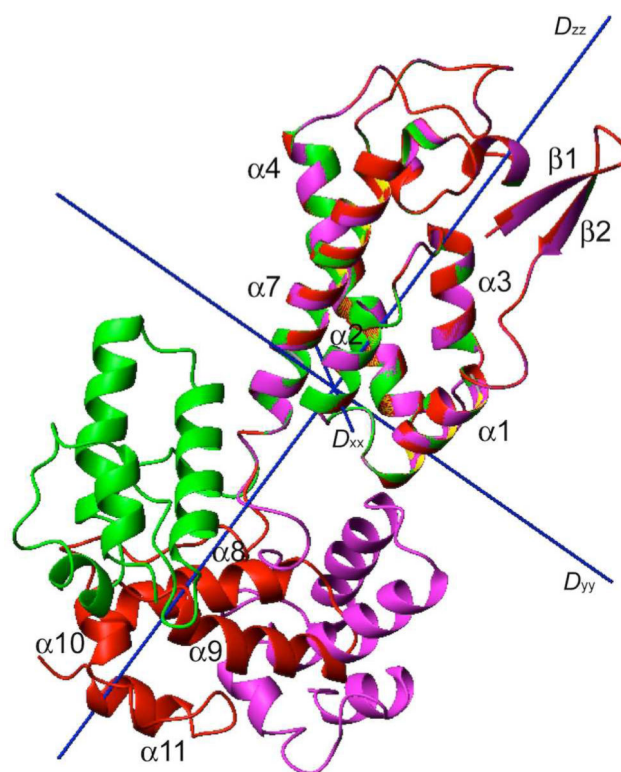


**Figure 4.** The alignment of domain CA<sup>N</sup> within the dual-domain EIAV-CA structure from the current  $T_1/T_2$  analysis (red), monomeric crystal structure (magenta, 2EIA-B), and a monomer within the HIV-1-CA hexamer crystal structure (green, 3GV2).

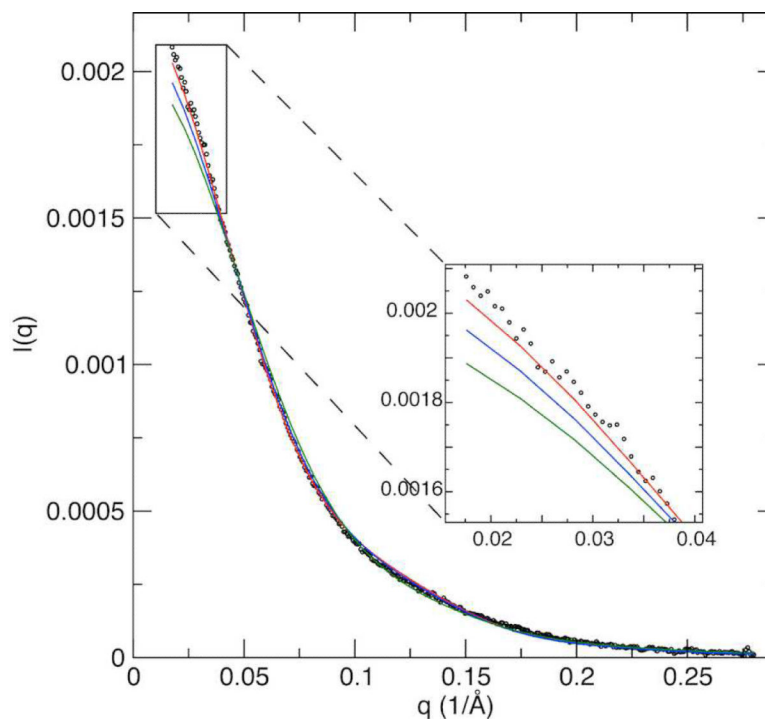


**Figure 5.** Experimental (dots) and fitting curves (solid) of small angle X-ray scattering. The structural coordinates of the current  $T_1/T_2$  determined (red), the monomeric EIAV-CA (2EIA, blue), and one monomer in hexameric HIV-1-CA (3GV2, green), were used for fittings. The EIAV-CA sample for SAXS measurement is 0.05 mM in the same buffer as NMR samples. Fitting of the structural coordinates were performed using XPLOR-NIH.(51)



Table 1

The extended model free fitting for  $^{15}\text{N}$   $T_1/T_2$  of EIAV-CA.

Concentration (mM)	Domain	$\tau_{\text{m}}^a$ (ns)	$2D_{zz}/(D_{yy}+D_{xx})$	$D_{yy}/D_{xx}$	$S^2$ domain	$\tau_{\text{domain}}$ (ns)	$\alpha$	$\beta$	$\gamma$	$\chi^2/N$
"0"	CAN	13.6	1.84	1.69	1.00	n/a	155°	112°	86.9°	15.6
	CAC				0.854	3.86	74.9°	18.7°	39.6°	
0.4	CAN	18.6	1.70	1.51	1.00	n/a	158°	112°	82.2°	60.9
	CAC				0.900	1.87	61.4°	18.2°	50.5°	

<sup>a</sup>  $\tau_{\text{m}}$  was calculated from  $1/(2D_{zz}+2D_{yy}+2D_{xx})$ .